ACOUSTIC SHADOWS DETECTION, APPLICATION TO ACCURATE RECONSTRUCTION OF $3D$ INTRAOPERATIVE ULTRASOUND

Pierre Hellier[1,2,3,5] *, Pierrick Coupé*[1,2,3]*, Pierre Meyer*[1,2,3]*, Xavier Morandi* [1,2,3,4] *and D.Louis Collins*[5]

[1] INRIA, VisAGeS U746 Unit/Project, IRISA, Campus de Beaulieu, F-35042 Rennes, France
[2] INSERM, VisAGeS U746 Unit/Project, IRISA, Campus de Beaulieu, F-35042 Rennes, France
[3] University of Rennes 1, CNRS, Campus de Beaulieu, F-35042 Rennes, France
[4] Service de neurochirurgie, Centre Hospitalier Régional Universitaire de Rennes, France
[5] Montreal Neurological Institute, McGill University, Montreal, Canada

ABSTRACT

Acoustic shadows appear in ultrasound images as regions of low signal intensity after boundaries with very high acoustic impedance differences. Acoustic shadows can be viewed as informative features to detect lesions or calcifications, or can be considered as damageable artifacts for image processing tasks such as segmentation, registration or $3D$ reconstruction. In both cases, the detection of these acoustic shadows is useful. This paper proposes a new geometrical method to detect these shadows based on statistical analysis of intensity profiles along the lines that compose the B-scan image. The results demonstrate that this detection improves the accuracy of $3D$ reconstruction of intraoperative ultrasound.

***Index Terms*—** Biomedical image processing, Biomedical acoustics, Image restoration

1. INTRODUCTION

The image formation process of ultrasound images is bound to the propagation and interaction of waves in tissues of various acoustic impedances. More precisely, at the boundary of two materials, the wave energy is transmitted, reflected, dispersed and/or diffracted. If the wave energy is almost totally reflected, this will result in an acoustic shadow in the region of the image beyond the boundary. The motivation for detecting acoustic shadows is twofold. First, the presence of an acoustic shadow reflects the presence of an interface where the acoustic energy was almost completely lost. This is typically an interface tissue/air or tissue/bone. Therefore, acoustic shadows can be used to detect lesions [1], calcifications, gallstones or bone structures. Second, acoustic shadows might limit the efficiency of image processing techniques like segmentation, registration [2, 3] or 3D reconstruction. This paper will focus on the impact of shadow estimation on image processing tasks and more precisely on $3D$ reconstruction of $2D$ tracked freehand ultrasound intraoperative data.

2. RELATED WORK

Only a few papers have presented methods to detect acoustic shadows. Methods can be broadly sorted in two groups: intensity-based methods [4, 1] and geometric methods [2, 3]. Intensity-based methods rely on a direct analysis of the intensities to detect dark regions. Madabhusi *et al.* [4] describe a method that combines a feature space extraction, manual training and classification to discriminate lesions from posterior acoustic shadowing. Drukker *et al.* [1] use a threshold on a local skewness map to detect shadows. Geometric methods take into account the probe's geometry and analyze intensity profiles along the lines that compose the B-scan. Leroy *et al.* [2] fit an heuristic exponential function to determine whether a shadow occured, while Penney *et al.* [3] manually estimate the image mask to determine dark areas. The method proposed in this paper belongs to the latter class of methods - geometrical methods. Contrary to previous papers, the image mask, the probe geometry and the statistical detection threshold are estimated automatically. Rather than fitting heuristic function to detect shadows, a statistical analysis is performed along each transducer line to detect potential shadows regions. The latter are modeled as ruptures (or breaks) along the intensity profiles coupled with a statistical noise test.

3. METHOD

3.1. Overview

Since the presence of acoustic shadows are bound to the geometry of the probe and to the propagation of the signal along the lines that compose the B-scan, it is necessary to estimate the probe's shape. Then, a signal analysis is performed along the lines that compose the B-scan. An acoustic shadow is detected along a line when two criteria are met: (1) a rupture along a line exists and (2) the signal distribution after the rupture is statistically compliant with an estimated noise model.

3.2. B-scan geometry extraction

Given a sequence of $2D$ ultrasound images (see a typical image in figure 1-**a**), it is necessary to separate the image and the background. This amounts to computing a $2D$ mask given the $2D + t$ sequence. To do so, maps of longitudinal mean and variance are computed, and multiplied pixelwise to compute a feature map. For a given point, the longitudinal mean is defined as the mean at a $2D$ pixel location over time. Background pixels are dark and have low (or zero) variance. Points in the image foreground have the highest values of the feature map (compared to the background). Then, points with the highest values of the feature map are retained (see figure 1-**b**). Some false detections exist, mainly due to textual data and complementary image information presented on the ultrasound machine display. Therefore, a morphological closing and opening are performed to clean the input mask (see figure 1-**c**). To estimate the probe geometry, a trapezoid model is fit to the input mask. The trapezoid model is the simplest model capable of capturing the geometry of a linear or curvilinear probe. The 5 parameters of the model are estimated by optimizing the total performance measure ϕ (see figure 1-**d**) that is defined as:

$$\phi = \frac{TP + TN}{TP + TN + FP + FN}' \tag{1}$$

where TP is the number of true positives, TN the number of true negatives, FP the number of false positives and FN the number of false negatives. For the model estimation, accuracy is needed for the extremal lines of the trapezoid. Several experiments were conducted with three different acquisition systems (various video acquisition cards and echographic machines) and demonstrated that the method performs robustly in all cases tested.

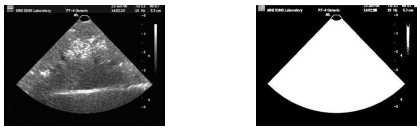

(a) Typical image (b) First mask

(c) Cleaned mask (d) Trapezoid estimation

Fig. 1. Illustration of the automatic mask extraction. (a) shows a typical image of the acquired sequence. (b) shows the first mask obtained after selecting the highest values of the longitudinal statistics. (c) shows the mask after morphological operators were applied to remove patient information. (d) shows the final trapezoid model estimation.

3.3. Line rupture detection

Once the probe's geometry is estimated, it is possible to know whether the direction of scanning is top-down or bottom-up when a curvilinear probe is used. For a linear probe, the user must specify the direction of scanning (it is generally top-down except if the video grabber flipped the image). Afterwards, it is necessary to sample line profiles corresponding to the transducer lines. For each B-scan, an arbitrary number of lines can be drawn and for each line, k samples are computed by trilinear interpolation in the corresponding B-scan. As mentionned previously, the shadow is defined as a signal rupture along the line, followed by a low signal afterwards. Therefore, signal ruptures are detected first. To do so, the line signal is smoothed with a low-pass filter. Then, a local symmetric entropy criterion is computed. For each point p of the line signal $\mathcal{S}$, a sliding window of size n is used to compute the rupture criterion $\mathcal{R}$:

$$\mathcal{R} = \sum_{i=1}^{i=n} \left(\mathcal{S}(p-i) \log \frac{\mathcal{S}(p-i)}{\mathcal{S}(p+i)} + \mathcal{S}(p+i) \log \frac{\mathcal{S}(p+i)}{\mathcal{S}(p-i)} \right)$$

The loci where $\mathcal{R}$ is maximal indicate a signal rupture. The rupture criterion $\mathcal{R}$ is quite general since it relies on the statistical dependency between the future and the past samples in a sliding window. Rupture positions are determined as zero-crossings of the gradient of $\mathcal{R}$. Figure 2 illustrates the rupture detection on a synthetic example.

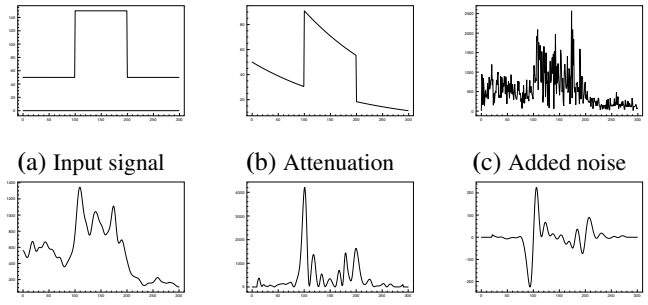

(a) Input signal (b) Attenuation (c) Added noise

(d) Filtered signal (e) Rupture detection (f) Rupture gradient

Fig. 2. Illustration of the line processing on a synthetic signal. (a): a synthetic ramp signal is used as an input. (b): an exponential attenuation is applied. (c): multiplicative Rayleigh noise is added. (d): the signal is smoothed with a low-pass filter. (e): the local rupture criterion $\mathcal{R}$ is computed, as well as its gradient in (f). All loci of a gradient zero-crossing are tested as possible candidates for a shadow detection.

3.4. Noise model and shadow detection

Each detected rupture is tested as a possible candidate for an acoustic shadow. To design the detection test, we rely on a

modeling of the ultrasound image statistics. Because of the difficulty to model the ultrasound image formation process, several models have been introduced so far. We use here a general model that has been successfully used for ultrasound images [5, 6, 7]. This model reads as:

$$u(x) = v(x) + \sqrt{v(x)} \cdot \mu(x) \text{ with } \mu(x) \sim \mathcal{N}(0, \sigma^2), \quad (2)$$

where u is the observed image and v the "ideal" signal. In this model, the noise depends on the signal intensity. In other words, the noise is higher in bright areas. We shall assume here that acoustic shadows are areas where the original signal v is constant with a relatively small value. When a rupture is detected and tested as a candidate for a shadow, let us denote $\mathbb{E}(u_f)$ (respectively $\mathbb{V}(u_f)$) the mean (respectively the variance) of the signal after the rupture. According to the noise model of equation 2, the shadow detection test reads as:

$$\mathbb{V}(u_f) < \mathbb{E}(u_f) \cdot \sigma^2. \quad (3)$$

We thus end up with estimating the parameter σ. To do so, we follow the approach described in [8]. On local square patches that intersect the B-scan mask, the local mean μ and variance ϑ are computed. The parameter σ can be interpreted as the linear regression parameter of the variance versus the mean: $\vartheta = \sigma^2 \cdot \mu + \epsilon$. This is true when patches are homogeneous, i.e. intersect only one anatomical tissue. This cannot be true in practice, as illustrated in figure 3-(a) where two regions R_1 and R_2 intersect the patch. Therefore, robust M-estimators are used to compute a robust mean and variance. The normal computation of local statistics is shown in figure 3-(b), while the robust computation of statistics is shown in figure 3-(c). From figure 3-(c), the linear regression is easily performed to determine automatically the parameter σ of the statistical shadow detection test.

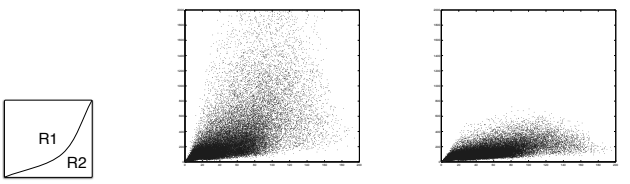

(a) Image patch (b) Raw regression (c) Robust regression

Fig. 3. Estimation of parameter σ of the noise model 2. On square patches, local statistics are computed to determine the parameter σ. Each dot represents the local statistic (variance on vertical axis versus mean on horizontal axis) of a single patch. Since a square patch cannot contain only one tissue, as illustrated on the left, robust statistics are used to compute the mean and variance. The use of robust statistics ((c)) enables a more accurate regression and estimation of σ compared to the regression using standard statistics ((b)).

3.5. Regularization

Since acoustic shadows are due to an anatomical structure that reflects the wave energy (which more precisely depends on the angle between the beam and the interface), the detection of acoustic shadows should vary smoothly between two consecutive lines. A simple regularization scheme is therefore adopted: for each line, the detection index is defined as the position of the detected shadow along the line. A median filtering of the detection indexes is performed on a local neighborhood of 10 adjacent lines to regularize the solution.

4. RESULTS

4.1. Material

The method was tested with $2D$ tracked freehand ultrasound images acquired during a neurosurgical procedure. The sonosite cranial $4-7MHz$ probe was tracked the Medtronic StealthStation© neuronavigation system. Ultrasound data were thus registered with the coordinate system of the preoperative Magnetic Resonance Images (MRI).

4.2. Detection of acoustic shadows

The estimation of acoustic shadows was tested on patient data with a brain cavernoma. In figure 4-**a**, a typical image of the sequence is shown. Figure 4-**b** and 4-**c** show the results of the shadow detection, without and with regularization respectively. For legibility, only a few lines were drawn. However, a dense estimation of the mask is performed by increasing the number of lines. The regularization removed false positive detections and smoothed the shape of the detected shadows. Regions of acoustic shadow and strong signal attenuation were detected by the method.

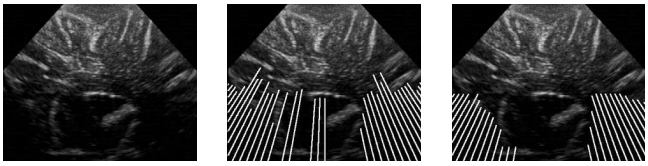

(a) Initial B-scan (b) Raw estimation (c) Regularized

Fig. 4. Example of shadow estimation on intraoperative brain ultrasound images. For legibility, only a few lines were sampled in this case. On the input B-scan (a), results of the shadow estimation are given without regularization (b) and after regularization (c). The regularization removes outliers and smoothes the profile of the shadow boundaries.

4.3. Impact on reconstruction

The impact of shadow detection was tested on a $3D$ reconstruction task. Given a sequence of $2D$ images and their $3D$

tracked positions and orientations, a regular $3D$ lattice volume can be reconstructed. The reconstruction method presented in [9] was used. In this experiment, the sequence was composed of two view points that differ mostly by a translation. Technically, areas detected as shadows regions were ignored in the distance-weighted interpolation step. Figure 5-a shows a slice of the initial reconstruction and 5-b is the reconstructed slice when taking into account the detection of acoustic shadows. Figure 5-c shows the corresponding pre-operative MR slice. Artifacts are visible, not only at the border between the two views, but also in deep regions. For instance, deep cerebral structures previously difficult to make out (lenticular nucleus and choroid plexus, see arrows) are clearly visble on the reconstructed US image when taking into account acoustic shadows. As a numerical assessment, the correlation ratio [10] was computed between the reconstructed US and the pre-operative MR. The correlation ratio increases from 0.15312 to 0.173996 when taking into account shadows, indicating objectively that the $3D$ reconstruction was improved.

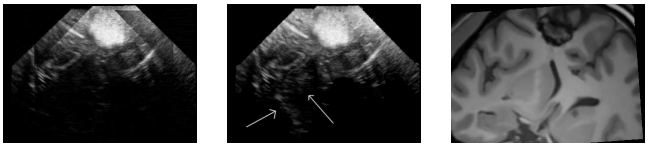

(a) Initial (b) Corrected (c) MR slice

Fig. 5. Impact of the shadow estimation on the reconstruction of $3D$ intraoperative brain ultrasound images. A sequence of $3D$ freehand ultrasound was acquired during brain surgery. During the sequence, two sweeps were done with different viewing angles. The two sweeps are compounded in one reconstructed volume. Image (a) shows a slice of the reconstructed volume with a Distance-Weighted reconstruction method. Reconstruction artifacts are visible on the boundaries of anatomical structures (sulci and cerebral falx). When incorporating the shadow estimation mask (figure (b)), artifacts are removed and deep structures appear clearly. The "border artifacts" at the left and right of the image are due to the B-scan mask that has been taken into account when reconstructing image (b).

5. CONCLUSION

We have presented an automatic method to detect shadows in ultrasound images that uses image statistics and regularization for accurate detection of shadow borders. Experiments using data from intraoperative brain ultrasound demonstrate that shadow detection leads to a more accurate 3D reconstruction when compounding US from two different view points. Further investigation will begin with the analysis of intensity attenuation within scans and between scans to distinguish the combined effects of anatomical structures, ultrasound machine settings such as gain or depth focus and include quantitative evaluation of the impact of shadow detection on registration, 3D reconstruction and structure segmentation. Furthermore, the tuning of the neighborhood size for regularization should be studied further and determined with respect to the scale of image structures.

6. REFERENCES

[1] Karen Drukker, Maryellen L. Giger, and Ellen B. Mendelson, "Computerized analysis of shadowing on breast ultrasound for improved lesion detection," *Medical Physics*, vol. 30, no. 7, pp. 1833–1842, 2003.

[2] Leroy A., Mozer P., Payan Y., and Troccaz J., "Rigid registration of freehand 3d ultrasound and CT-scan kidney images," in *MICCAI*, 2004, LNCS 3216, pp. 837–844.

[3] G.P. Penney, J.M. Blackall, M.S. Hamady, T. Sabharwal, A. Adam, and D.J. Hawkes, "Registration of freehand 3d ultrasound and magnetic resonance liver images," *Medical Image Analysis*, vol. 8, pp. 81–91, 2004.

[4] A. Madabhusi, P. Yang, M. Rosen, and S. Weinstein, "Distinguishing lesions from posterior acoustic shadowing in breast ultrasound via non-linear dimensionality reduction," in *EMBS*, 2006, pp. 3070–3073.

[5] Xiaohui Hao, Shangkai Gao, and Xiaorong Gao, "A novel multiscale nonlinear thresholding method for ultrasonic speckle suppressing," *IEEE Transactions on Medical Imaging*, vol. 18, no. 9, pp. 787–794, 1999.

[6] Krissian K., Vosburgh K., Kikinis R., and Westin C.-F., "Speckle-contrained anisotropic diffusion for ultrasound images," in *CVPR*, 2005, pp. 547–552.

[7] T. Loupas, W. N. McDicken, and P. L. Allan, "An adaptive weighted median filter for speckle suppression in medical ultrasonic images," *IEEE transactions on Circuits and Systems*, vol. 36, no. 1, pp. 129–135, 1989.

[8] K. Hirakawa and T. W. Parks, "Image denoising using total least squares," *IEEE Transactions on Image Processing*, vol. 15, no. 9, pp. 2730–2742, 2006.

[9] P Coupe, P Hellier, X Morandi, and C Barillot, "Probe trajectory interpolation for 3d reconstruction of freehand ultrasound.," *Medical Image Analysis*, vol. 11, no. 6, pp. 604–615, 2007.

[10] A. Roche, G. Malandain, and N Ayache, "Unifying maximum likelihood approaches in medical image registration," *International Journal of Imaging Systems and Technology*, vol. 11, no. 1, pp. 71–80, 2000.